

NUMERICAL SIMULATION OF GLUEY PARTICLES

ALINE LEFEBVRE¹

ABSTRACT. We propose here a model and a numerical scheme to compute the motion of rigid particles interacting through the lubrication force. In the case of a particle approaching a plane, we propose an algorithm and prove its convergence towards the solutions to the gluey particle model described in [19]. We propose a multi-particle version of this gluey model which is based on the projection of the velocities onto a set of admissible velocities. Then, we describe a multi-particle algorithm for the simulation of such systems and present numerical results.

RÉSUMÉ. Nous proposons ici un modèle ainsi qu'un schéma numérique afin de résoudre le mouvement de particules rigides en interaction à travers la force de lubrification. Dans le cas d'une particule à l'approche d'un plan, nous proposons un algorithme et montrons sa convergence vers le modèle de particules visqueuses décrit dans [19]. Nous proposons une version multi-particules de ce modèle qui est basée sur la projection des vitesses sur un espace de vitesses admissibles. Ensuite, nous décrivons un algorithme multi-particules pour la simulation de tels systèmes et présentons des résultats numériques.

1. INTRODUCTION

Slurries, lava's flows or red cells in blood are systems made of rigid particles embedded in viscous fluids (if we consider as a first approximation that red blood cells are rigid). Such systems can also be found in industry: concrete, paper pulp or some food industry products. These systems present varieties of noticeable rheological behaviours, whose study has been the subject of a great amount of researches, with contributions coming from engineering, chemistry, physics or mathematics. The basic problem is to predict macroscopic transport properties of these suspensions – viscosity, settling velocity – from microstructures, that is to say, from the interactions between particles and from their spatial configuration.

In case of dilute suspensions, theoretical results come from neglecting near field interactions. For example, in 1906, Einstein proposed an asymptotic formula for the apparent viscosity of dilute suspensions [5]. In that case, apparent viscosity only depends on the solid volume fraction. Unfortunately, agreement between such asymptotic results and experiments generally fails as soon as the solid fraction reaches a few percent. For higher solid fractions, near field interactions can not be neglected anymore and it becomes essential to take them into account. Note that, studying the behaviour of neighbouring particles is of great interest, not only to understand the behaviour of dense suspensions, but also to study the fluid/particle system of equations modelling suspensions of particles. Indeed, existence of solutions to these equations has been proved as long as the distance remains strictly positive (see for example [4, 24, 25]). Global weak solutions have also been constructed in [6, 22], supposing that solids

Key words and phrases. fluid/particle systems, fluid/solid interaction, lubrication force, contacts, Stokes fluid.

1. Laboratoire de Mathématiques, Université Paris-Sud, 91405 Orsay Cedex, France, aline.lefebvre@math.u-psud.fr.

stick after contact. However, nothing is said concerning the possibility that such a contact may occur in finite time. A good understanding of near field interactions is therefore necessary to study more precisely these systems.

These interactions between solids embedded in a viscous fluid are due to lubrication forces: for the solids to get very close, the fluid must be evacuated from the narrow gap between them, which creates a force penalizing their relative motion. This force is singular in the distance and this singularity is sufficient to avoid contacts. Indeed, it has been proved in [9] that in two dimensions, a smooth particle embedded in a viscous fluid following Navier-Stokes equations can not touch a plane in finite time. This behaviour can be recovered from the asymptotic expansion of the lubrication force, available for a Stokes fluid in three dimensions (see [1] for example):

$$(1) \quad \mathbf{F}_{lub} \sim -6\pi\mu r^2 \frac{\dot{q}}{q},$$

where μ is the viscosity of the fluid, r the radius of the particle and q the distance between the particle and the plane. Indeed, using this first order approximation, we can write the Fundamental Principle of Dynamics for a particle of mass m submitted to an external force f :

$$(2) \quad m\ddot{q}(t) = -6\pi\mu r^2 \frac{\dot{q}}{q} + mf(t),$$

and the fact that the maximal solution to this ODE is global and never goes to zero (contact) in finite time comes from the Cauchy-Lipschitz theorem. Similarly, in case of a fixed sphere of radius r_1 and another sphere of radius r_2 moving at velocity \mathbf{V} along the axe of the centers, the first term of the developpement of the lubrication force exerted on the moving particle is (see [2]):

$$(3) \quad \mathbf{F}_{lub} \sim -6\pi\mu \frac{r_1^2 r_2^2}{(r_1 + r_2)^2} \frac{\mathbf{V}}{q},$$

and no contact can occur in finite time.

This force, while acting at microscopic level, can be very important for the macroscopic behaviour of the global system, especially in case of high density of particles. Even for Stokes flows, it induces complexity and nonlinearity. This complex link between microscopic and macroscopic levels makes it difficult to obtain theoretical results and studying these systems requires numerical simulations. In order to obtain relevant simulations for dense suspensions, the lubrication force has to be taken into account with accuracy. However, direct numerical simulation induces space discretization which makes it difficult to solve accurately the fluid in the narrow gap between neighbouring particles. As a consequence, numerical contacts can be observed in such simulations and physical reasons as well as numerical robustness make it necessary to develop specific technics to deal with these contacts.

A first idea to solve this problem is to search for a strategy allowing an accurate computation of the lubrication forces. In [10], a method based on local refinements of the space and time meshes is proposed, so that the lubrication force in the interparticle gap is taken into account with accuracy and prevents overlappings. However, the number of refinements needed is not known a priori and the method can become computationally heavy. Consequently, less time-consuming methods have been developed. Some of them consist in adding a short range repulsive force (see [7, 21] or [27]). In [17] a minimizing algorithm is used to impose a minimal distance between the particles, while in [23], the particles are allowed to undergo slight overlappings and an elastic repulsive force is added when

such overlappings are detected. All of these methods ensure numerical robustness but introduce new parameters and do not take into account the underlying physics. Another approach is to use inelastic collisions. This idea has been proposed in [11] in order to impose a minimal distance between the particles. In [18], a scheme for inelastic collisions, based on a global projection step of the velocities, has been developed for granular flows and makes it possible to handle lots of particles. This scheme has been coupled with a fluid/particle solver in [13], to avoid contacts. More physical strategies, taking the lubrication force into account, have finally been proposed. Each of them relies on the asymptotic development of the lubrication force (3). In [3, 20], it is shown that these lubrication forces are solution to a linear system. They are computed at each time step and added to the simulations. Unfortunately, this leads to stiff systems and, whereas it better takes into account the underlying physics, contact problems still occur because of the time discretization. In [16] a method is proposed to stabilize this problem by computing accurately sensible quantities such as the interparticle distances. However, a projection step is still needed for big time steps, in order to avoid overlappings.

The purpose of this article is to propose a strategy dealing simultaneously with contacts and lubrication forces. We restrict ourself here to the study of a gluey contact model without taking the surrounding fluid into account. This model is based on the gluey particle one described in [19]. We propose an algorithm for this particle/plane model and prove its convergence. Then, we generalize it to the multi-particle case. The numerical strategy is to combine the algorithm given for the plane/particle case with the scheme proposed in [18] for granular flows. While programming this multi-particle algorithm, we watched out for dealing with contacts efficiently in order to manage to simulate collections of many particles. Numerical simulations for few thousands of gluey particles are presented in the last section. An example of coupling with a fluid/particle solver is given in section 2.4 in the particle/plane case.

2. SINGLE PARTICLE ABOVE A PLANE

2.1. The gluey particle model. We consider a three-dimensional spherical particle moving perpendicularly to a plane (See Fig. 1). Its velocity and radius are denoted by \mathbf{V} and r respectively. Its distance to the plane is q .

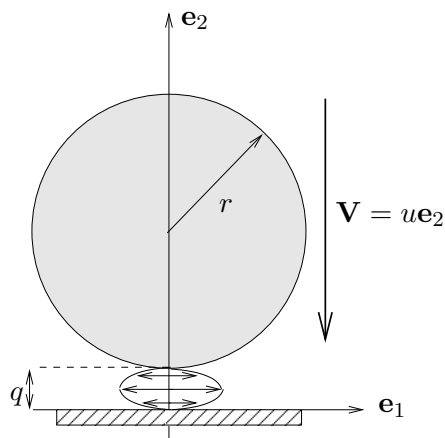


FIGURE 1. Notations.

The gluey particle model has been proposed in [19]. It describes, from a macroscopic point of view, the behaviour of the system near contact. It is built as the vanishing viscosity limit of the lubrication model (1) and relies on two states, glued ($q = 0$) or unglued ($q > 0$). These states are described by a new variable γ which stands for an adhesion potential: the more γ is negative, the more the solids are glued.

We denote by $I =]0, T[$ the time interval. The unknowns q and γ belong to the following functional spaces:

$$q \in W^{1,\infty}(I), \quad \dot{q} \in BV(I), \quad \gamma \in BV(I),$$

and the initial conditions are:

$$q(0) = q^0 > 0, \quad \dot{q}(0) = u^0, \quad \gamma(0) = 0.$$

In order to be able to generalize the model to the multi-particle case, we use the following second order ODE formulation given in [19]:

$$(4) \quad \dot{q}(t^+) = \Pi_{C_{q,\gamma}(t)} \dot{q}(t^-),$$

$$(5) \quad m\ddot{q} = mf + \lambda \text{ in } \mathcal{M}(I) = (\mathcal{C}_c(I))',$$

$$(6) \quad \text{supp}(\lambda) \subset \{t, q(t) = 0\},$$

$$(7) \quad \dot{\gamma} = -\lambda,$$

$$(8) \quad q \geq 0, \quad \gamma \leq 0,$$

where $C_{q,\gamma}(t)$ is the set of admissible velocities at time t :

$$C_{q,\gamma}(t) = \begin{cases} \{0\} & \text{if } \gamma(t^-) < 0, \\ \mathbb{R}^+ & \text{if } \gamma(t^-) = 0, \quad q(t) = 0, \\ \mathbb{R} & \text{else.} \end{cases}$$

Remark 2.1. In this formulation, \dot{q} and γ are supposed to be in $BV(I)$. In order to alleviate the notations, their differential measures have been denoted by \ddot{q} and $\dot{\gamma}$ respectively.

The behaviour of the solutions to this problem is the following. By (5) and (6), q is solution to $\ddot{q} = f$ while there is no contact ($q > 0$). Suppose a collision occurs at time t_0 , we have $\dot{q}(t_0^-) < 0$ and $\gamma(t_0^-) = 0$. Then $C_{q,\gamma}(t_0)$ is \mathbb{R}^+ and (4) gives $\dot{q}(t_0^+) = 0$. By (5), we obtain that, in the sense of distributions, λ identifies to the dirac mass at time t_0 weighted by the velocity jump $m(\dot{q}(t_0^+) - \dot{q}(t_0^-)) = -m\dot{q}(t_0^-)$. This, together with (7) finally gives that γ is initialized to the value $m\dot{q}(t_0^-) < 0$. From then, while γ remains strictly negative, $C_{q,\gamma}$ is reduced to $\{0\}$ and, combining this with (4) gives that there is adhesion between the solids ($q = 0$). During this adhesion, \ddot{q} is zero and therefore, (7) associated to (5) gives $\dot{\gamma} = mf$. By definition of $C_{q,\gamma}$, the particle is allowed to take off when γ is back to zero. An example of such a behaviour is given in figure 2

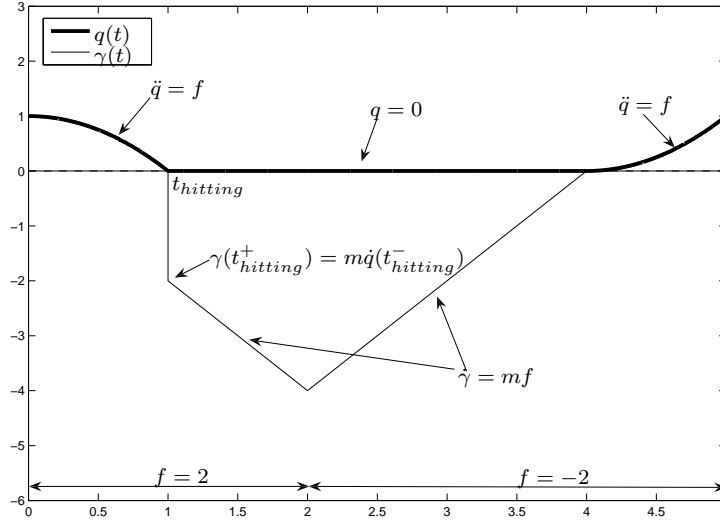


FIGURE 2. Example of solution to the gluey particle model.

Remark 2.2. The additional constraints (8) are necessary. Indeed, suppose that t_1 is an unsticky contact time ($q(t_1) = 0$, $\gamma(t_1^-) = 0$, $\dot{q}(t_1^-) = 0$). If the force is negative after this instant and if we do not impose $q \geq 0$, then $\gamma \equiv 0$ and $\dot{q}(t) = \int_{t_1}^t f(s)ds$ is a solution to the problem and the particle can enter the wall. Similarly, if the force is positive and if the constraint $\gamma \geq 0$ is not imposed, $q \equiv 0$ and $\gamma(t) = m \int_{t_1}^t f(s)ds$ is a solution and γ can become strictly positive.

Before proposing an algorithm to compute the solutions to this model, we make a few remarks about its interpretation and its physical relevance.

Remark 2.3 (Physical interpretation). As already mentioned, a smooth particle embedded in a newtonian fluid never touches the plane in finite time. In the context of the gluey particle model, the variable q can be seen as a macroscopic distance between the solids: it is equal to zero as soon as the solids are near contact. The new variable γ , which is obtained as the limit of $\gamma_\mu = \mu \ln(q)$, stands for the microscopic distance. To understand the behaviour of the gluey particle system presented on figure 2, one can consider a rigid ball falling on a table coated with a viscous fluid like honey. When the particle reaches the layer of fluid, it instantaneously sinks in it and the depth it reaches is linked to the impact velocity. From then, the ball is glued to the layer of fluid, the macroscopic contact begins, q is set to zero and γ stores the impact velocity. As long as it is pushed, the particle sinks deeper in the fluid and gets closer to the plane (γ decreases). Then the particle is pulled. From that moment on, it smoothly moves back from the fluid (γ increases) and comes unstuck from the layer of fluid when the pulling forces have balanced the impact velocity and the pushing forces (γ reaches zero). Note that, from (5), λ can be interpreted as an additional force, exerted by the plane on the particle, in order to satisfy the constraint (4). It follows from (6) that the plane is allowed to act on the particle through this force only if they are in macroscopic contact.

Remark 2.4 (Radius). This gluey particle model is built in [19] as the vanishing viscosity limit of the lubrication model (1) where each constant except the viscosity is taken equal to 1. Taking all

constants into account leads to define γ as the limit of $\gamma_\mu = 6\pi\mu l n(q)$ and the equation governing its evolution becomes

$$(9) \quad \dot{\gamma} = -\frac{1}{r^2}\lambda.$$

The larger r is, the less the microscopic distance γ varies (the more it is difficult for the particle to move). Note that, provided we are only interested in the macroscopic trajectory q of the particle, the previous model (4)-(8) was valid for any radius: these trajectories only depend on the sign of γ (and not its value) which is independent of r from (9).

Remark 2.5 (Viscous or not viscous ?). Since this model is built by letting the viscosity go to zero, one may wonder whether it models viscous fluids or not. To answer this question, we consider the same experiment as in figure 2 (pushing until time 2 and then pulling) for a particle falling on a plane coated with different viscous fluids. On figure 3, we compare the trajectory given by the gluey particle model to the trajectories computed for these systems where the viscous fluid layer is modeled by (2). Of course, trajectories converge to the limit model when the viscosity goes to zero. We also

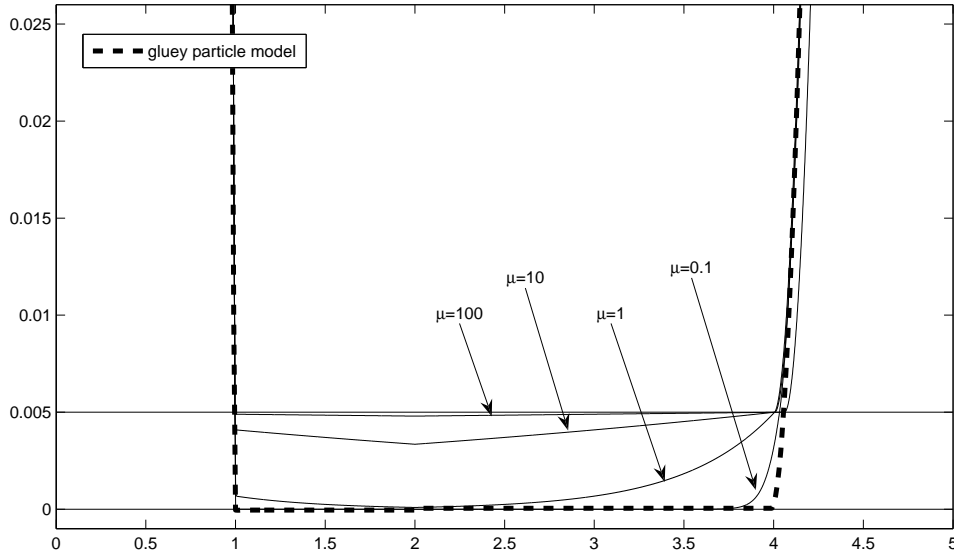


FIGURE 3. Comparison gluey particle model / layer of viscous fluid.

observe that, from a macroscopic point of view, as long as we are interested in hitting and unsticking times, the limit model seems to agree with all trajectories. As a matter of fact, from this point of view, what is important is not the viscosity of the fluid but whether it is viscous or not. However, the main difference between the trajectories is the minimal distance reached by the particle. Actually, small viscosities induce very small distances and, consequently, the system can reach a domain wherein the initial lubrication model (2) is no longer valid. To conclude, the gluey particle model shall be employed to represent the macroscopic behaviour of very viscous systems for which distances are not too small.

2.2. Numerical algorithm. We propose here an algorithm for problem (4)-(8). Let $h = T/N$ be the time step. The problem is initialized to $q^0 > 0$, $u^0 \in \mathbb{R}$ and $\gamma^0 = \lambda^0 = 0$. We denote by q^n , u^n , γ^n and λ^n the computed values of q , u , γ and λ at time t^n . We define f^n by $f^n = \frac{1}{h} \int_{t^n}^{t^{n+1}} f(s) ds$. We have to compute q^{n+1} , u^{n+1} , γ^{n+1} and λ^{n+1} .

In order to compute u^{n+1} and λ^{n+1} , we define the discrete counterpart of $C_{q,\gamma}(t^n)$ the following way:

$$\left\{ \begin{array}{l} K(q^n, \gamma^n) = \{v, q^n + hv \geq 0\} \text{ if } \gamma^n = 0, \\ K(q^n, \gamma^n) = \{v, q^n + hv = 0\} \text{ if } \gamma^n < 0. \end{array} \right.$$

$K(q^n, \gamma^n)$ is called the set of admissible velocities at time t^n . The collision law (4) and the Fundamental Principle of Dynamics (5) then become,

$$\left\{ \begin{array}{l} u^{n+1/2} = u^n + hf^n, \\ u^{n+1} \in K(q^n, \gamma^n), \quad \frac{1}{2} |u^{n+1} - u^{n+1/2}|_m^2 = \min_{v \in K(q^n, \gamma^n)} \frac{1}{2} |v - u^{n+1/2}|_m^2, \end{array} \right.$$

where $(v, w)_m = (mv, w)$. Note that $u^{n+1/2}$ is the velocity the particle would have at time t^{n+1} if there were no plane. u^{n+1} is the projection of this a priori velocity on the set of admissible velocities $K(q^n, \gamma^n)$ for an adapted scalar product. From this projection step, arises a Lagrange multiplier, denoted by λ^{n+1} (positive if $\gamma^n \geq 0$), and such that

$$m(u^{n+1} - u^{n+1/2}) = h\lambda^{n+1}.$$

This can be rewritten as

$$(10) \quad m \frac{u^{n+1} - u^n}{h} = mf^n + \lambda^{n+1},$$

which is a discretization of (5).

Then, γ^{n+1} is given by an explicit Euler discretization of (7),

$$\gamma^{n+1} = \gamma^n - h\lambda^{n+1}.$$

This equation is valid while γ^{n+1} is negative. If it becomes strictly positive, it means that the particle has taken off at a time $t^* \in]t_n, t_{n+1}[$. In that instance, γ^{n+1}/m has integrated the force on $]t^*, t^{n+1}[$ instead of u^{n+1} which was fixed to zero. Therefore, in that case, we modify u^{n+1} and γ^{n+1} the following way :

$$\text{if } \gamma^{n+1} > 0, \quad u^{n+1} = \gamma^{n+1}/m \text{ and } \gamma^{n+1} = 0.$$

Finally the position q^{n+1} is given by

$$q^{n+1} = q^n + hu^{n+1}.$$

To sum up, the algorithm is the following :

Algorithm 2.6 (Particle/plane). For all $n \geq 0$, let q^n , u^n , γ^n and λ^n be given. We define $f^n = \frac{1}{h} \int_{t^n}^{t^{n+1}} f(s) ds$.

- (1) Computation of the a priori velocity, without taking the lubrication force into account

$$u^{n+1/2} = u^n + hf^n.$$

- (2) Projection of the a priori velocity onto the set of admissible velocities,

$$\bar{u}^{n+1} \in K(q^n, \gamma^n), \quad \frac{1}{2} \left| \bar{u}^{n+1} - u^{n+1/2} \right|_m^2 = \min_{v \in K(q^n, \gamma^n)} \frac{1}{2} \left| v - u^{n+1/2} \right|_m^2,$$

where $K(q, \gamma) = \{v, q + hv \geq 0\}$ if $\gamma = 0$,

$K(q, \gamma) = \{v, q + hv = 0\}$ if $\gamma < 0$.

From this projection step, we obtain λ^{n+1} .

- (3) Updating of γ ,

$$\bar{\gamma}^{n+1} = \gamma^n - h\lambda^{n+1}.$$

- (4) Modification if unsticking,

$$\begin{aligned} \text{if } \bar{\gamma}^{n+1} \leq 0, \quad u^{n+1} &= \bar{u}^{n+1} & \text{and} \quad \gamma^{n+1} &= \bar{\gamma}^{n+1}, \\ \text{if } \bar{\gamma}^{n+1} > 0, \quad u^{n+1} &= \bar{\gamma}^{n+1}/m & \text{and} \quad \gamma^{n+1} &= 0. \end{aligned}$$

- (5) Updating of q ,

$$q^{n+1} = q^n + hu^{n+1}.$$

Remark 2.7 (Coupling with fluid simulations). This algorithm simulates collections of gluey particles. Let us now suppose that the particles are embedded in a viscous fluid. To make simulations taking the lubrication force into account, a splitting method can be used to couple a fluid/particle solver with the gluey particle algorithm. We denote by \mathbf{u}^n and p^n the velocity and pressure fields into the fluid at time t^n . Let S be any fluid/particle solver: from \mathbf{u}^n , q^n and f^n , S computes the a priori velocities of the particles, without taking the lubrication force into account carefully. To couple the two algorithms we propose to modify step (1) of algorithm 2.6 writing:

$$u^{n+1/2} = S(q^n, \mathbf{u}^n, f^n).$$

2.3. Convergence result. In this section, we establish a convergence result for the proposed algorithm. To begin, we rewrite problem (4)-(8) as

$$(11) \quad \begin{cases} m\dot{q} + \gamma = m \left(\dot{q}(0) + \int_0^t f(s) ds \right), \\ q \geq 0, \quad \gamma \leq 0, \quad q\gamma = 0, \\ q(0) = q^0 > 0, \quad \dot{q}(0) = u^0, \end{cases}$$

which is formally equivalent to the previous one (see [19]).

We recall that h is the constant time step. We denote by q_h the piecewise affine function with $q_h(t^n) = q^n$. Similarly, γ_h is the piecewise affine function with $\gamma_h(t^n) = \gamma^n$. We denote by u_h the

derivative of q_h , piecewise constant equal to u^{n+1} on $]t^n, t^{n+1}[$. Finally, we define $\lambda_h = -\dot{\gamma}_h$, piecewise constant. Note that, due to step (4), λ_h is generally not equal to λ^{n+1} on $]t^n, t^{n+1}[$. We will denote by $\tilde{\lambda}^{n+1} = -(\gamma^{n+1} - \gamma^n)/h$ its value on this interval. If the particle does not take off between times t^n and t^{n+1} , no modification is made during step (4) and we obtain $\tilde{\lambda}^{n+1} = \lambda^{n+1}$. The convergence theorem is the following:

Theorem 2.8. *Let f be integrable on $I =]0, T[$. When h goes to zero, there exists subsequences, still denoted by $(q_h)_h$, $(u_h)_h$, $(\lambda_h)_h$ and $(\gamma_h)_h$, $q \in W^{1,1}(I) \cap \mathcal{C}(I)$ and $\gamma \in BV(I)$ such that*

$$\begin{aligned} u_h &\longrightarrow u \text{ in } L^1(I), \\ q_h &\longrightarrow q \text{ in } W^{1,1}(I) \text{ and } L^\infty(I) \text{ with } \dot{q} = u, \\ \lambda_h &\xrightarrow{*} \lambda \text{ in } \mathcal{M}(I), \\ \gamma_h &\longrightarrow \gamma \text{ in } L^1(I) \text{ with } \dot{\gamma} = -\lambda, \end{aligned}$$

where (q, γ) is solution to (11).

Remark 2.9. Non-uniqueness for the limit problem (see [19] for counter-example) prevents from using the standard approach based on consistence and stability. Consequently, we use compactness methods and obtain convergence up to subsequences. However, in case q has a finite number of zeros, the limit model admits a unique solution and therefore the convergence of the algorithm to problem (11) is proved. Moreover, in that case, it can be shown that (4)-(8) and (11) are equivalent, in the sense that a solution to one of the problem is also solution to the other (the demonstration of this result can be found in [14]). Consequently, under the a priori hypothesis that q has a finite number of zeros, theorem 2.8 shows that algorithm 2.6 converges to (4)-(8). For example, this hypothesis is verified if the external force f changes of sign a finite number of times.

Proof of theorem 2.8

To begin, note that a discrete form of the Fundamental Principle of Dynamics (5) is verified:

$$(12) \quad \forall n, \quad m \frac{u^{n+1} - u^n}{h} = m f^n + \tilde{\lambda}^{n+1}.$$

Indeed, in case the particle does not take off between times t^n and t^{n+1} , the equality follows from (10), together with $\tilde{\lambda}^{n+1} = \lambda^{n+1}$. If the particle takes off, it comes from (10) and step 4 of the algorithm.

The proof will be divided into 4 steps.

(1) Convergence of q_h and u_h

Lemma 2.10. *$(u_h)_h$ is bounded in $L^\infty(I)$.*

Proof : In case the particle does not take off, the projection step (2) gives

$$|u^{n+1}| = |\bar{u}^{n+1}| \leq |u^{n+1/2}| \leq |u^n| + h|f^n|.$$

In the other case, it can be proved that $u^{n+1} \tilde{\lambda}^{n+1} \leq 0$ and combining this with (12) gives the same result. By summing up all these inequalities we obtain

$$|u^{n+1}| \leq |u^0| + \int_0^T |f|,$$

and the result follows from definition of u_h . \square

Lemma 2.11. $(u_h)_h$ is bounded in $BV(I)$.

Proof : By lemma 2.10, the result will follow provided we prove $\text{Var}(u_h)$ is bounded independently from h , where

$$\text{Var}(u_h) = \sum_{n=1}^{N-1} |u^{n+1} - u^n|.$$

To check this, we first split the sum and consider the sums between indexes p_1 and n_1 where t^{p_1} and t^{n_1} are successive unsticking times (See Fig. 4):

$$\text{Var}_{[t^{p_1}, t^{n_1}[}(u_h) = \sum_{n=p_1}^{n_1-1} |u^{n+1} - u^n|.$$

The total variation of u_h is made of a sum of such terms.

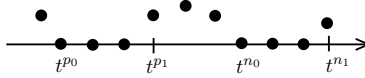


FIGURE 4. Proof of lemma 2.11 : notations.

The idea behind the above decomposition is that, at each unsticking time t^{p_1} , the velocity of the particle is small and that its variations over $[t^{p_1}, t^{n_1}[$ only depend on the integral of f over the same interval. These terms will be summed up to obtain a bound on the total variation.

More precisely, the bound for $\text{Var}_{[t^{p_1}, t^{n_1}[}(u_h)$ can be found by analysing each jump $|u^{n+1} - u^n|$, paying attention to what happens at time t^n (hitting time, sticking time, unsticking time). For the sake of readability, details of the computation are skipped here, they can be found in [14]. We find

$$\text{Var}_{[t^{p_1}, t^{n_1}[}(u_h) \leq 4 \int_{t^{p_1-1}}^{t^{n_1}} |f(s)| ds.$$

Summing up all these contributions and the bounding terms, we obtain

$$\text{Var}(u_h) \leq u^0 + 8 \int_0^T |f(s)| ds,$$

and $\text{Var}(u_h)$ is bounded independently from h as required. \square

Lemma 2.11, together with the compact embedding of $BV(I)$ in $L^1(I)$ gives (up to a subsequence)

$$(13) \quad \begin{aligned} u_h &\longrightarrow u \text{ in } L^1(I) \text{ with } u \in BV(I), \\ q_h &\longrightarrow q \text{ in } W^{1,1}(I) \text{ with } \dot{q} = u. \end{aligned}$$

Uniform convergence of q_h to q then follows from the continuous embedding of $W^{1,1}(I)$ in $L^\infty(I)$:

$$(14) \quad q_h \longrightarrow q \text{ in } L^\infty(I).$$

Finally, since q_h is positive, we have $q \geq 0$ everywhere.

(2) **Convergence of γ_h**

Lemma 2.12. $(\lambda_h)_h$ is bounded in $L^1(I)$.

Proof : By (12) and the fact that $\tilde{\lambda}^0 = 0$ we get

$$\int_0^T |\lambda_h| \leq m \text{Var}(u_h) + \|f\|_{L^1(I)}.$$

The result follows by combining this with lemma 2.11. \square

By lemma 2.12, $(\lambda_h)_h$ is bounded in $\mathcal{M}(I)$, which implies that there exists a subsequence and $\lambda \in \mathcal{M}(I)$ such that

$$\lambda_h \xrightarrow{*} \lambda \text{ in } \mathcal{M}(I).$$

Moreover, combining lemma 2.12 with $\dot{\gamma}_h = -\lambda_h$ it comes that $(\gamma_h)_h$ is bounded in $BV(I)$. This, together with compact embedding of $BV(I)$ in $L^1(I)$, implies that there exists a subsequence and $\gamma \in BV(I)$ such that

$$(15) \quad \gamma_h \rightarrow \gamma \text{ in } L^1(I) \text{ and a.e.}$$

Since γ_h is negative, it follows from this convergence result that so is γ . Finally, since $\dot{\gamma}_h = -\lambda_h$, we can check that $\dot{\gamma} = -\lambda$ in $\mathcal{M}(I)$.

 (3) **Continuous FPD**

We are now going to prove that $m\dot{q} + \gamma = m \left(\dot{q}(0) + \int_0^t f(s)ds \right)$ almost everywhere on I .

In order to do so, the first step is to prove that (5) is verified in the sense of distributions. From (12) it follows that

$$(16) \quad \forall \varphi \in \mathcal{D}(I), \quad \langle m\dot{u}_h, \varphi \rangle = \sum_{n=1}^{N-1} mh f^n \varphi(t^n) + \sum_{n=1}^{N-1} h \tilde{\lambda}^{n+1} \varphi(t^n).$$

We are going to pass to the limit in this equation. By (13), $\langle m\dot{u}_h, \varphi \rangle$ converges to $\langle m\dot{u}, \varphi \rangle$. To study the first term of the right-hand side, we write

$$h \sum_{n=1}^{N-1} f^n \varphi(t^n) = \int_0^T f(s) \varphi(s) ds + \sum_{n=1}^{N-1} \int_{t^n}^{t^{n+1}} f(s) [\varphi(t^n) - \varphi(s)] ds - \int_{t^0}^{t^1} f(s) \varphi(s) ds.$$

The convergence to zero of the sum over n comes from uniform continuity of φ . Combining this with $|t^1 - t^0| = h$ gives

$$\sum_{n=1}^{N-1} mh f^n \varphi(t^n) \rightarrow m \int_0^T f(s) \varphi(s) ds \text{ when } h \rightarrow 0.$$

The argument for the last term is similar. We write

$$\sum_{n=1}^{N-1} h \tilde{\lambda}^{n+1} \varphi(t^n) = \int_0^T \lambda_h(s) \varphi(s) ds + \sum_{n=1}^{N-1} \int_{t^n}^{t^{n+1}} \lambda_h(s) [\varphi(t^n) - \varphi(s)] ds - \int_{t^0}^{t^1} \lambda_h(s) \varphi(s) ds.$$

The convergence to zero of the sum over n comes from uniform continuity of φ and lemma 2.12, and the last term is equal to zero for all h . This, together with lemma 2.12 gives

$$\sum_{n=1}^{N-1} h\tilde{\lambda}^{n+1}\varphi(t^n) \longrightarrow \langle \lambda, \varphi \rangle = -\langle \dot{\gamma}, \varphi \rangle \text{ when } h \rightarrow 0.$$

Finally, passing to the limit in (16) we obtain

$$\langle m\ddot{q} - \dot{\gamma}, \varphi \rangle = \langle mf, \varphi \rangle, \quad \forall \varphi \in \mathcal{D}(I),$$

as required.

Then, by density of $\mathcal{D}(I)$ in $\mathcal{C}_0^0(I)$ and the fact that $m\dot{q} - \gamma$ is in $BV(I)$, we get

$$m\ddot{q} - \dot{\gamma} = mf \text{ in } \mathcal{M}(I).$$

Integrating this equality over $[0, t[$ (Stieltjes integral of BV functions) we obtain

$$(m\dot{q} - \gamma)(t^+) - (m\dot{q} - \gamma)(0^-) = \int_0^t mf,$$

and the result follows from this, by using $\gamma(0^-) = 0$ and a.e. continuity of $m\dot{q} - \gamma$.

(4) **Proof of $q\gamma = 0$**

To prove that (q, γ) is solution to (11), it remains to show that $q\gamma = 0$ almost everywhere. For all n we have $q^n\gamma^n = 0$. However, $q_h\gamma_h$ is not identically equal to zero. We build new functions \tilde{q}_h and $\tilde{\gamma}_h$, piecewise constant, with respective values q^n and γ^n on $]t^n, t^{n+1}[$. We now have $\tilde{q}_h\tilde{\gamma}_h = 0$ and simple computations give

$$\|\tilde{q}_h - q\|_{L^\infty(I)} \leq \|\tilde{q}_h - q_h\|_{L^\infty(I)} + \|q_h - q\|_{L^\infty(I)} \leq h\|u_h\|_{L^\infty(I)} + \|q_h - q\|_{L^\infty(I)}$$

and

$$\|\tilde{\gamma}_h - \gamma\|_{L^1(I)} \leq \|\tilde{\gamma}_h - \gamma_h\|_{L^1(I)} + \|\gamma_h - \gamma\|_{L^1(I)} \leq \frac{h}{2}\|\lambda_h\|_{L^1(I)} + \|\gamma_h - \gamma\|_{L^1(I)}.$$

Combining the first inequality with lemma 2.10 and (14) gives uniform convergence of \tilde{q}_h to q . Putting together the second inequality, lemma 2.12 and (15), we see that $\tilde{\gamma}_h$ converges to γ in $L^1(I)$ which implies that the sequence converges up to a subsequence almost everywhere on I . Finally, letting h go to zero in $\tilde{q}_h\tilde{\gamma}_h = 0$ gives $q\gamma = 0$ almost everywhere as required.

This completes the proof of theorem 2.8. \square

2.4. Validation: coupling with a fluid/particle solver. We consider the same experiment that the one considered in section 2, without inertia. The radius of the particle is taken equal to 1 and the viscosity of the fluid is $\mu = 3$. The balance of forces reads

$$(17) \quad \forall t, \quad F_{lub}(q(t)) + f(t) = 0,$$

where $f(t) = -2$ until time 2 and $f(t) = 2$ if $t > 2$.

To obtain a reference solution we first compute, as accurately as possible, the map $q \rightarrow F_{lub, u_0}(q)$ for a given velocity $u_0 = -1$ and $q \in [0, 1]$. To do so, we begin with computing $F_{lub, u_0}(q_k)$ where $(q_k)_{k=1..M}$ is a regular subdivision of interval $[0, 1]$. This is done, for each q_k , solving the Stokes problem in the fluid with Dirichlet boundary conditions and computing the force $F_{lub, u_0}(q_k)$ exerted by the fluid on the particle. The computations are carried out in tree-dimensions using an axisymmetric formulation

and the Finite-Element solver **FreeFem++**. On the left side of figure 5, we plot the numerical results obtained (circles). They agree with the asymptotic expansion (1) for small distances (solid line). Finally, the map $q \rightarrow F_{lub}(q)$ is approximated using a least square approximation of the numerical results by a polynomial of degree 3 (dashed line).

The reference solution is obtained discretizing the time interval and computing the velocity of the particle u^n at each time-step. We write that $u^n = \alpha^n u_0$ and, using the linearity of the lubrication force with respect to the velocity, we compute α^n as the solution to

$$\alpha^n F_{lub,u_0}(q^n) + f(t^n) = 0.$$

The trajectory obtained is plotted against time on the right side of figure 5.

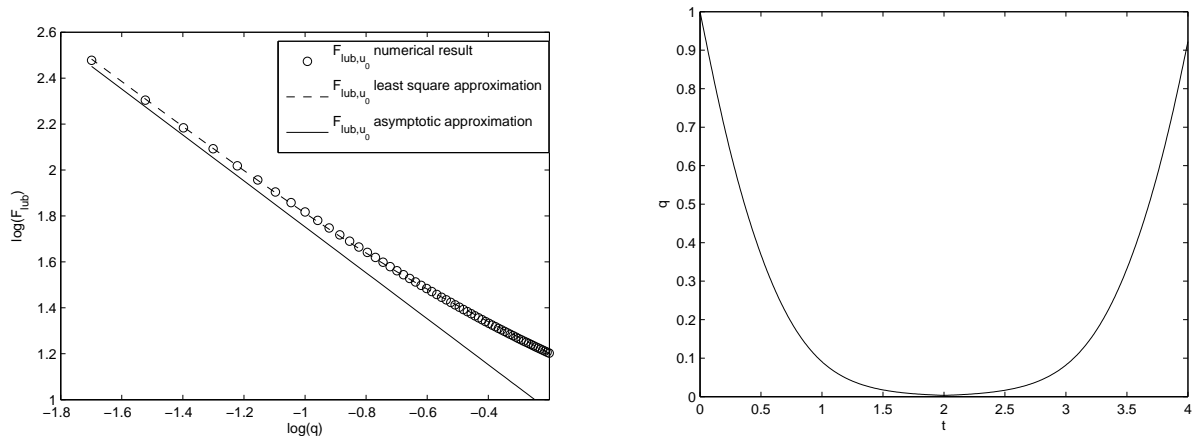


FIGURE 5. Approximation of the lubrication force (left) and reference solution (right).

We now want to observe the influence of the method employed to deal with contacts in fluid/particle simulations. To do so, we use an axisymmetrical version of the fluid/particle solver implemented with **FreeFem++** and described in [13]. On figure 6, we plot the solution given by this solver for a mesh size $\delta x = r/10$ (dashed line). We can observe that the particle remains glued. Indeed, due to the space discretization, the characteristic function representing the rigid particle ends up with touching the boundary of the domain and the Dirichlet boundary condition prevents it from taking off. Consequently, it is necessary to deal with the problem of contact and to prevent the characteristic function from intersecting the boundary of the domain. Two methods are tested: the fluid/particle solver is coupled with an inelastic contact algorithm and with the gluey contact model. The coupling is performed using the splitting strategy described in remark 2.7. In each case, the constraint for the distance is set to $q \geq \eta$ with $\eta = \delta x$. The numerical results are compared on figure 6. We observe that, for the inelastic model (solid line with crosses), the particle takes off as soon as it is pulled. To the contrary, using the gluey contact model (solid line with circles), the particle remains glued and the trajectory finally joins up with the reference one. This is a validation of the gluey particle model and it emphasizes the necessity to take the lubrication force into account when dealing with contacts.

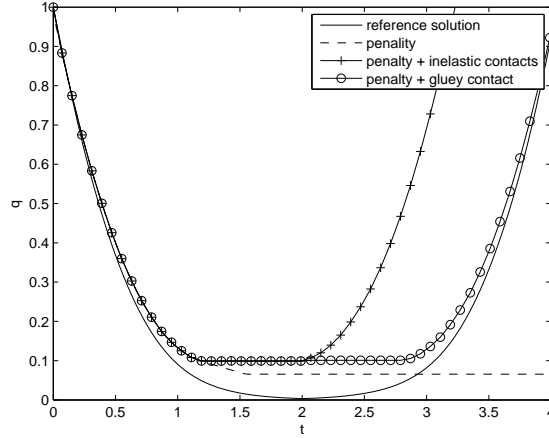


FIGURE 6. Comparison of the numerical solutions for different contact models.

Finally, we observe on figure 7 the behaviour of the two contact models with respect to the parameter η which is the minimal distance allowed between the particle and the plane. We can see that the trajectories obtained for different η separates after unsticking time when using the inelastic contact model (left side of the figure). This is due to the fact that, for this model, the particle unsticks as soon as it is pulled. To the contrary, the gluey particle model is not so sensible to parameter η (right side of the figure).

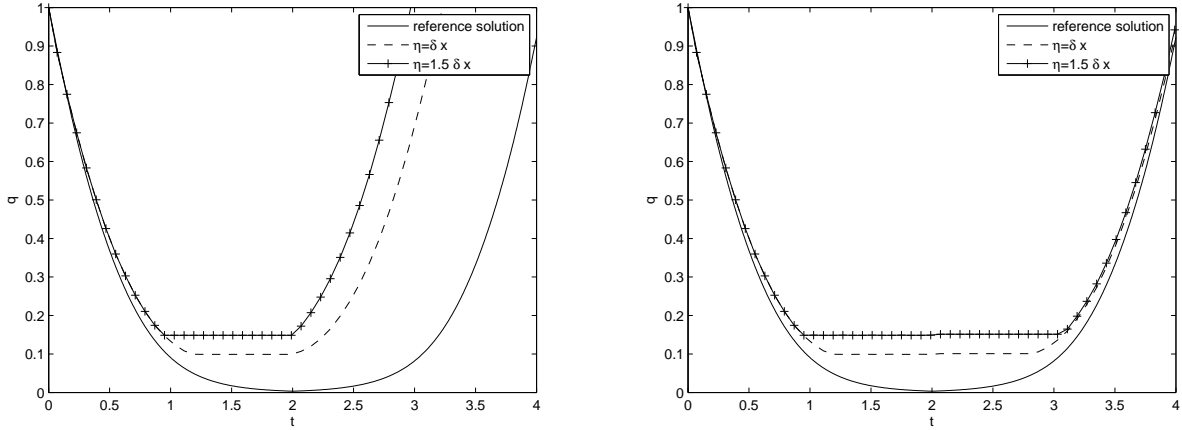


FIGURE 7. Impact of η on the numerical solution for inelastic (left) and gluey (right) contact.

2.5. Extension to rough solid surfaces. As already said, it has been proved that smooth solids can not undergo contact. However, from our experience, we know that the particle should touch the plane in finite time. One of the reasons explaining this behaviour is that physical particles are not smooth. Recent experiments described in [26] show that the lubrication force exerted on a rough

particle is the one would be exerted on a shifted smooth particle:

$$(18) \quad F_{lub,rough} \sim -6\pi\mu r^2 \frac{\mathbf{V}}{q + q_s},$$

where $q_s < r_s$ (see Fig. 8). Due to the lubrication force, this equivalent smooth sphere can not undergo

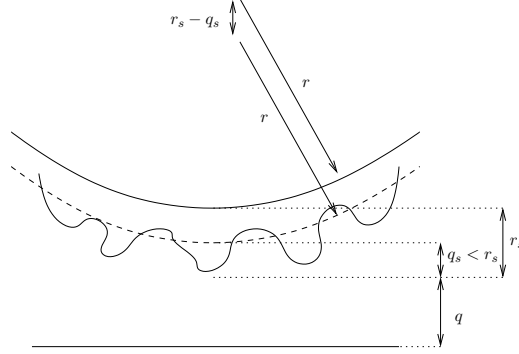


FIGURE 8. Equivalent smooth sphere.

contact with the plane ($q + q_s$ doesn't go to zero in finite time) but the real surfaces can collide (q can go to zero).

Taking these results into account in the gluey particle model, we consider that, as soon as $q = r_{1,s} + r_{2,s}$ (see notations on figure 9), there exists a real solid/solid contact. During this contact, the forces acting on the particle are not registered anymore. To model such a behaviour, it suffices to recall that γ is the limit of $\gamma_\mu = 6\pi\mu l n(q_\mu)$ (see remark 2.4) and to impose

$$\gamma \geq 6\pi\mu l n(r_{s,1} + r_{s,2}).$$

The trajectory computed for this model is plot on figure 9. We can observe that the rough particle takes off before the smooth one. Contrary to what has been said in remark 2.4 for the smooth case,

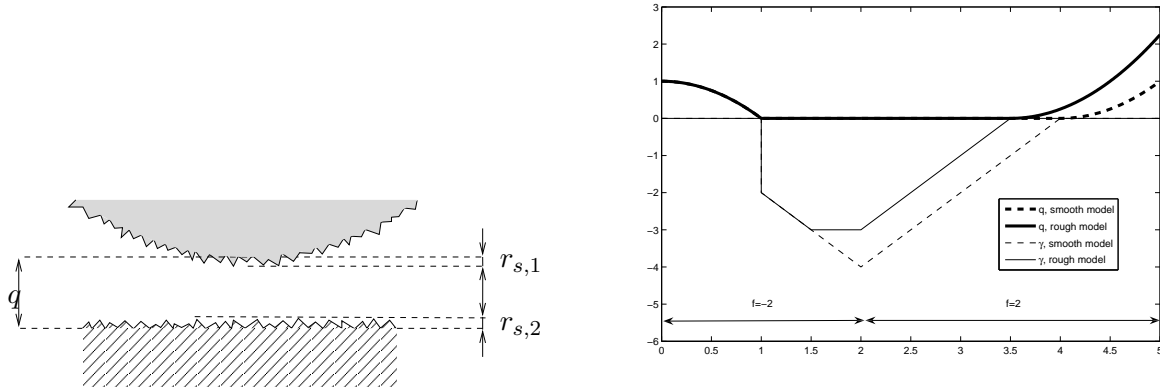


FIGURE 9. Rough solids: notations (left) and gluey particle model (right).

it is now important to know the value of γ in order to truncate it. Therefore, it is essential to take

the radius into account in its evolution and to use equation (9) in the gluey particle model:

$$\dot{\gamma} = -\frac{1}{r^2}\lambda.$$

In that case, the trajectory of the particle depends on r .

From an algorithmic point of view, this rough model can easily be taken into account in algorithm 2.6 by changing step (3) in

$$\gamma^{n+1} = \gamma^n - \frac{h}{r^2}\lambda^{n+1},$$

where r is the radius of the sphere and by adding the following (4b) step:

$$\text{if } \gamma^{n+1} < \gamma_{min}, \quad \gamma^{n+1} = \gamma_{min}.$$

3. MULTI-PARTICLE CASE

3.1. Modelling. We generalize the gluey particle model (4)-(8) to the multi-particle case. We consider a system of N spherical particles in three-dimensions. \mathbf{x}_i stands for the position of the center of particle i in \mathbb{R}^3 and $\mathbf{f}_i \in \mathbb{R}^3$ for the external force exerted on it. Let $\mathbf{x} \in \mathbb{R}^{3N}$ be defined by $\mathbf{x} = (\dots, \mathbf{x}_i, \dots)$ and $\mathbf{f} \in \mathbb{R}^{3N}$ by $\mathbf{f} = (\dots, \mathbf{f}_i, \dots)$. We denote by D_{ij} the signed distance between particles i and j , and \mathbf{e}_{ij} by $\mathbf{e}_{ij}(\mathbf{x}) = (\mathbf{x}_j - \mathbf{x}_i) / \|\mathbf{x}_j - \mathbf{x}_i\|$ (see Fig. 10). We define M as the mass matrix of dimension $3N \times 3N$, $M = \text{diag}(\dots, m_i, m_i, m_i, \dots)$. Vector $\mathbf{G}_{ij} \in \mathbb{R}^{3N}$ is the gradient of distance D_{ij} with respect to the positions of the particles:

$$\mathbf{G}_{ij}(\mathbf{x}) = \nabla_{\mathbf{x}} D_{ij}(\mathbf{x}) = (\dots, 0, \underbrace{-\mathbf{e}_{ij}(\mathbf{x})}_i, 0, \dots, 0, \underbrace{\mathbf{e}_{ij}(\mathbf{x})}_j, 0, \dots, 0)^t.$$

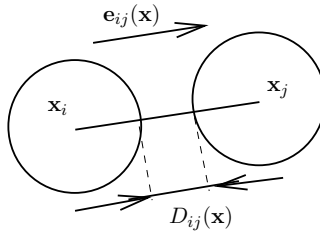


FIGURE 10. Particles i et j : notations.

In that context, there are $N(N-1)/2$ pair of particles and we denote by $\boldsymbol{\gamma} = (\dots, \gamma_{ij}, \dots) \in \mathbb{R}^{N(N-1)/2}$ the associated sticking variables: γ_{ij} is strictly negative if particles i and j are glued. Then, using the fact that $\frac{dD_{ij}(\mathbf{x})}{dt} = \mathbf{G}_{ij}(\mathbf{x}) \cdot \dot{\mathbf{x}}$, we define the following space of admissible velocities:

$$C_{\mathbf{x}, \boldsymbol{\gamma}}(t) = \left\{ \mathbf{V} \in \mathbb{R}^{3N} \text{ s.t. } \left| \begin{array}{l} \mathbf{G}_{ij}(\mathbf{x}) \cdot \mathbf{V} = 0 \text{ if } \gamma_{ij}(t^-) < 0 \\ \mathbf{G}_{ij}(\mathbf{x}) \cdot \mathbf{V} \geq 0 \text{ if } \gamma_{ij}(t^-) = 0, D_{ij}(t) = 0 \end{array} \right. \right\}.$$

To finish with notations, we denote by $\boldsymbol{\lambda} = (\dots, \lambda_{ij}, \dots) \in \mathbb{R}^{N(N-1)/2}$ the vector made of the Lagrange multipliers associated to these $N(N-1)/2$ constraints.

The multi-particle model is the natural counterpart of the particle/plane one:

$$(19) \quad \left\{ \begin{array}{l} \mathbf{x} \in (W^{1,\infty}(I))^{3N}, \quad \dot{\mathbf{x}} \in (BV(I))^{3N}, \quad \gamma \in (BV(I))^{N(N-1)/2}, \quad \boldsymbol{\lambda} \in (\mathcal{M}(I))^{N(N-1)/2}, \\ \dot{\mathbf{x}}(t^+) = P_{C_{\mathbf{x},\gamma}(t)} \dot{\mathbf{x}}(t^-), \\ M\ddot{\mathbf{x}} = M\mathbf{f} + \sum_{i < j} \lambda_{ij} \mathbf{G}_{ij}(\mathbf{x}), \\ \text{supp}(\lambda_{ij}) \subset \{t, D_{ij}(t) = 0\} \text{ for all } i, j, \\ \dot{\gamma} = -\boldsymbol{\lambda}, \\ D_{ij} \geq 0, \quad \gamma_{ij} \leq 0 \text{ for all } i, j, \\ \mathbf{x}(0) = \mathbf{x}^0 \text{ st. } D_{ij}(0) > 0 \text{ for all } i, j, \quad \dot{\mathbf{x}}(0) = \mathbf{u}^0, \quad \gamma(0) = 0_{\mathbb{R}^{N(N-1)/2}}. \end{array} \right.$$

Remark 3.1. The Lagrange multiplier λ_{ij} , associated to the constraint between particles i and j , is activated (non zero) only if these particles are in contact. The additional force due to this contact is equal to $\lambda_{ij} \mathbf{G}_{ij}(\mathbf{x})$. From the expression of $\mathbf{G}_{ij}(\mathbf{x})$, we get that this force only concerns the particles involved in the contact: it is equal to $-\lambda_{ij} \mathbf{e}_{ij}(\mathbf{x})$ on particle i and $\lambda_{ij} \mathbf{e}_{ij}(\mathbf{x})$ on particle j .

Remark 3.2 (Roughness and radius). As for the particle/plane case (see section 2.5), roughness can be taken into account by imposing a threshold on γ :

$$6\pi\mu l n(r_{i,s} + r_{j,s}) \leq \gamma_{ij} \text{ for all } i, j,$$

where $r_{l,s}$ is the size of roughness of particle l . As noticed in the particle/plane case, it is now important to take the radius of the particles into account in the evolution of γ . To do so, in the same way as in the particle/plane case, we come back to the way the gluey particle model has been built and take into account all the constants involved in the first order asymptotic developpement of the lubrication force exerted between two particles (3). We obtain the following evolution equation for γ :

$$\dot{\gamma} = -R\boldsymbol{\lambda},$$

where R is the diagonal matrix of dimension $N(N-1)/2$ with coefficients $R_{ij,ij} = (r_i + r_j)^2 / (r_i^2 r_j^2)$.

3.2. Algorithm. Let h be the time step. We denote by $\mathbf{V}^n = (\dots, \mathbf{V}_i^n, \dots) \in \mathbb{R}^{3N}$ the approximated velocities of the particles at time $t^n = nh$. Let \mathbf{x}^n , γ^n and $\boldsymbol{\lambda}^n$ be the respective approximations of \mathbf{x} , γ and $\boldsymbol{\lambda}$ at time t^n .

The discretization of the continuous constraints $C_{\mathbf{x},\gamma}(t^n)$ is inspired by [18] and corresponds to a first order approximation of the constraints:

$$K(\mathbf{x}^n, \gamma^n) = \left\{ \mathbf{V} \in \mathbb{R}^{3N} \text{ s.t. } \left\{ \begin{array}{l} D_{ij}(\mathbf{x}^n) + h\mathbf{G}_{ij}(\mathbf{x}^n) \cdot \mathbf{V} \geq 0 \text{ if } \gamma_{ij}^n = 0 \\ D_{ij}(\mathbf{x}^n) + h\mathbf{G}_{ij}(\mathbf{x}^n) \cdot \mathbf{V} = 0 \text{ if } \gamma_{ij}^n < 0 \end{array} \right. \right\}.$$

Using this discrete space of admissible velocities, the time discretization of (19) is now a direct adaptation of algorithm 2.6 to the multi-particle case.

Algorithm 3.3 (Multi-particle). For all $n \geq 0$, let \mathbf{x}^n , \mathbf{V}^n , γ^n and $\boldsymbol{\lambda}^n$ be given. We define $\mathbf{f}^n = \frac{1}{h} \int_{t^n}^{t^{n+1}} \mathbf{f}(s) ds$.

(1) Computation of the a priori velocity, without taking the lubrication force into account

$$\mathbf{V}^{n+1/2} = \mathbf{V}^n + h\mathbf{f}^n.$$

(2) Projection of the a priori velocity on the set of admissible velocities,

$$\mathbf{V}^{n+1} \in K(\mathbf{x}^n, \gamma^n), \quad \frac{1}{2} \left| \mathbf{V}^{n+1} - \mathbf{V}^{n+1/2} \right|_M^2 = \min_{\mathbf{V} \in K(\mathbf{x}^n, \gamma^n)} \frac{1}{2} \left| \mathbf{V} - \mathbf{V}^{n+1/2} \right|_M^2.$$

From this projection step, we obtain $\boldsymbol{\lambda}^{n+1}$.

(3) Updating of γ ,

$$\begin{aligned} \gamma^{n+1} &= \gamma^n - h\boldsymbol{\lambda}^{n+1}, \\ \text{if } \gamma_{ij}^{n+1} &> 0, \quad \gamma_{ij}^{n+1} = 0. \end{aligned}$$

(4) Updating of \mathbf{x} ,

$$\mathbf{x}^{n+1} = \mathbf{x}^n + h\mathbf{V}^{n+1}.$$

Remark 3.4. In the same way as in section 2.5 and remark 2.7 for the particle/plane case, this algorithm can be extended to rough solids and coupled with fluid/particle solvers using a splitting strategy.

Remark 3.5 (Obstacles). Suppose there exists N_0 fixed obstacles (walls of a box containing the particles for example). It is straightforward to add the NN_0 new constraints in $K(\mathbf{x}^n, \gamma^n)$. Now, suppose these obstacles are moving with a prescribed velocity. We denote by \mathbf{y}^{n+1} the (known) vector giving their position at time t^{n+1} . The space of admissible velocities becomes:

$$K(\mathbf{x}^n, \mathbf{y}^{n+1}, \gamma^n) = \left\{ \mathbf{V} \in \mathbb{R}^{3N} \text{ s.t. } \left. \begin{array}{l} \text{Pairs } (i, j) \text{ particle/particle :} \\ D_{ij}(\mathbf{x}^n) + h\mathbf{G}_{ij}(\mathbf{x}^n) \cdot \mathbf{V} \geq 0 \text{ if } \gamma_{ij}^n = 0 \\ D_{ij}(\mathbf{x}^n) + h\mathbf{G}_{ij}(\mathbf{x}^n) \cdot \mathbf{V} = 0 \text{ if } \gamma_{ij}^n < 0 \\ \text{Pairs } (i, k) \text{ particle/obstacle :} \\ D_{ik}(\mathbf{x}^n, \mathbf{y}^{n+1}) + h\mathbf{G}_{ik}(\mathbf{x}^n, \mathbf{y}^{n+1}) \cdot \mathbf{V} \geq 0 \text{ if } \gamma_{ik}^n = 0 \\ D_{ik}(\mathbf{x}^n, \mathbf{y}^{n+1}) + h\mathbf{G}_{ik}(\mathbf{x}^n, \mathbf{y}^{n+1}) \cdot \mathbf{V} = 0 \text{ if } \gamma_{ik}^n < 0 \end{array} \right\}.$$

3.3. Finding neighbours. The most time consuming step in algorithm 3.3 is the projection step (2). It is performed using a Uzawa algorithm which imposes to run matrix/vector products involving the contacts. However, in order to simulate large collections of particles, it is essential to avoid loops over the $N(N-1)/2$ possible contacts. To do so, we notice that it is not necessary to take into account all contacts at each time-step. Indeed, two particles i and j far enough to each other at time t^n won't stick at time t^{n+1} and consequently, the corresponding constraint won't be activated (ie. $\lambda_{ij}^{n+1} = 0$). We denote by D_{neigh} the distance above which we consider that two particles are not likely to touch next time-step. Then, the set of pairs of particles one has to consider at time t^n is:

$$C_{neigh}(\mathbf{x}^n) = \{(i, j) \in [1, N]^2, \quad i < j \text{ and } D_{ij}(\mathbf{x}^n) \leq D_{neigh}\}.$$

If the pair (i, j) is in the set $C_{neigh}(\mathbf{x}^n)$, we say that particles i and j are neighbours. Two particles that are not neighbours at time t^n won't stick at time t^{n+1} and consequently, one can restrict the set of constraints at time t^n to:

$$K_{neigh}(\mathbf{x}^n, \gamma^n) = \left\{ \begin{array}{l} \mathbf{V} \in \mathbb{R}^{3N} \text{ s.t. , } \forall (i, j) \in C_{neigh}(\mathbf{x}^n) , \\ \left| \begin{array}{l} D_{ij}(\mathbf{x}^n) + h\mathbf{G}_{ij}(\mathbf{x}^n) \cdot \mathbf{V} \geq 0 \text{ if } \gamma_{ij}^n \geq 0 \\ D_{ij}(\mathbf{x}^n) + h\mathbf{G}_{ij}(\mathbf{x}^n) \cdot \mathbf{V} = 0 \text{ if } \gamma_{ij}^n < 0 \end{array} \right. \end{array} \right\}.$$

Remark 3.6. This idea not to take into account particles far away from each other is generally used when considering particles interacting through near field interaction forces, decreasing with the distance. In that case, it consists in considering that the force is negligible above a certain distance and consequently, it is an approximation of the model. In our case, no approximation is made. Indeed, if D_{neigh} has been chosen sufficiently large, we know that the pairs of particles that are not belonging to $C_{neigh}(\mathbf{x}^n)$ won't interact at time t^{n+1} . For example, we can choose a time step in order to limit the displacement of the particles to twice their radius and then set the value of D_{neigh} to a few radiuses.

To construct $C_{neigh}(\mathbf{x}^n)$ avoiding the computation of the $N(N-1)/2$ distances, we choose a bucket sorting type algorithm. It consists in dividing the computational domain into boxes of size $\nu > D_{neigh}$ and to compute distances only for pairs of particles belonging to neighbouring boxes (see Fig. 11). Note that, because of step (3), it is not sufficient to erase at each time-step the former set of neighbours

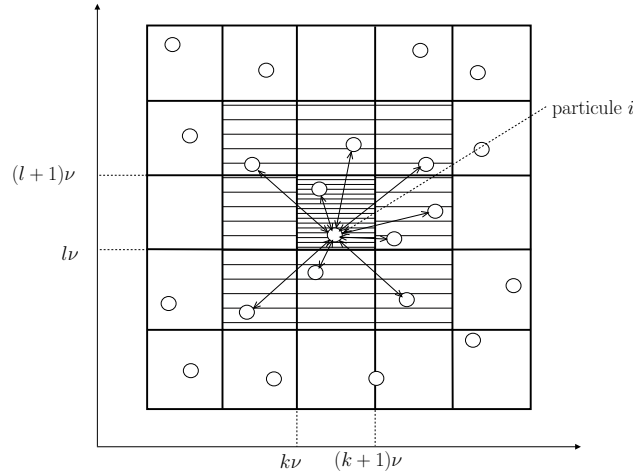


FIGURE 11. Algorithm to find neighbours: neighbouring boxes and distances actually computed.

and to create the new one: one has to transfer the value of γ_{ij}^n if particles i and j are in contact during these two successive time steps.

3.4. Object Oriented Programming Method. To build this code, we chose to use the object oriented programming method for mathematical problems CsiMoon [12]. As a consequence, both numerical methods and models can be easily changed. For example, new methods can be chosen and added to the code in order to perform the projection step and to construct the set of neighbours. This programming method also allows us to take into account various models of external environment (dry environment, fluid, obstacles of different shapes...), of interparticular interactions (cohesion force...)

and of contacts (inelastic, gluey model, aggregation...). This leads to a modular C++ code SCoPI [15], allowing Simulations of Collections of Interacting Particles. This code has already been used to simulate gluey particles, crowd motion, wet particles and red-cells (as an assembly of rigid particles).

4. NUMERICAL SIMULATIONS

We present in this section numerical simulations of collections of gluey particles. For visualization reasons, we only propose here two-dimensional simulations: even though the code is intrinsically three-dimensional, the motion of the particles is restricted to a vertical plane. These simulations demonstrate that the algorithm enables to take great numbers of gluey particles into account. This, together with section 2.4, shows that coupling the gluey particle algorithm with fluid/particle solvers will make it possible to simulate dense fluid/particle flows, taking the lubrication force into account with accuracy.

4.1. Gluey lotto: influence of roughness. The aim of this simulation is to observe the influence of roughness on the behaviour of multi-particle systems governed by the gluey particle model. We consider a two-dimensional “gluey lotto” made of 160 particles in a squared rotating mixer operator. The side length of the box is 0.5 and the radiuses of the particles are taken between 0.007 and 0.015. All particles have the same mass $m = 1$ and the gravity constant g is taken equal to 10. The 80 particles initially situated in the left compartment of the box are black and the 80 other ones are white. We represent side by side on figure 12 the configurations obtained at different time steps for $\gamma_{min} = 0$ on the left (inelastic contacts), $\gamma_{min} = -1$ in the middle (gluey rough particles) and $\gamma_{min} = -\infty$ on the right (gluey smooth particles). In case of smooth particles, the heaps of particles take off from the wall when they are at the top of the box: as suggested by the particle/plane model, they take off only when the gravity has balanced the forces it has itself exerted to push the particles on the bottom wall. In the rough case, they take off earlier.

4.2. Sedimentation of 3000 gluey particles. We consider 3000 gluey particles sedimenting under gravity with radiuses between 0.015 and 0.025. They are initially situated above a funnel (random sample of positions) with velocity equal to zero. All the particles have the same mass $m = 2$ and the gravity g is taken equal to 10. Below the funnel, a wheel rotates around its axis with angular velocity $\omega = -2$ and throws the particles on a leaning fixed plane situated below it. Then, the particles slip along the plane and finally fall in a container. Some spherical obstacles of radius $r = 0.1$ are fixed on the plane to slow the particles movement. A threshold is imposed on γ ($\gamma \geq -10$) to model roughness. Snapshots of this simulation are presented for different time-steps on figure 13. The code also allows us to model dry granular flow involving inelastic contacts. In figure 14 we compare the configurations obtained at the same time-step for such a simulation and the previous gluey one. Finally, we plot on figure 15 the values of γ for a given configuration of the gluey simulation. For each contact, a tube is plotted between the two involved particles and, the larger is γ_{ij} (ie. the more the particles are glued), the more the grey is dark. We can see the network of the forces leading to a packed configuration in the funnel. The particles are smoothly unsticking from each other when leaving the wheel.

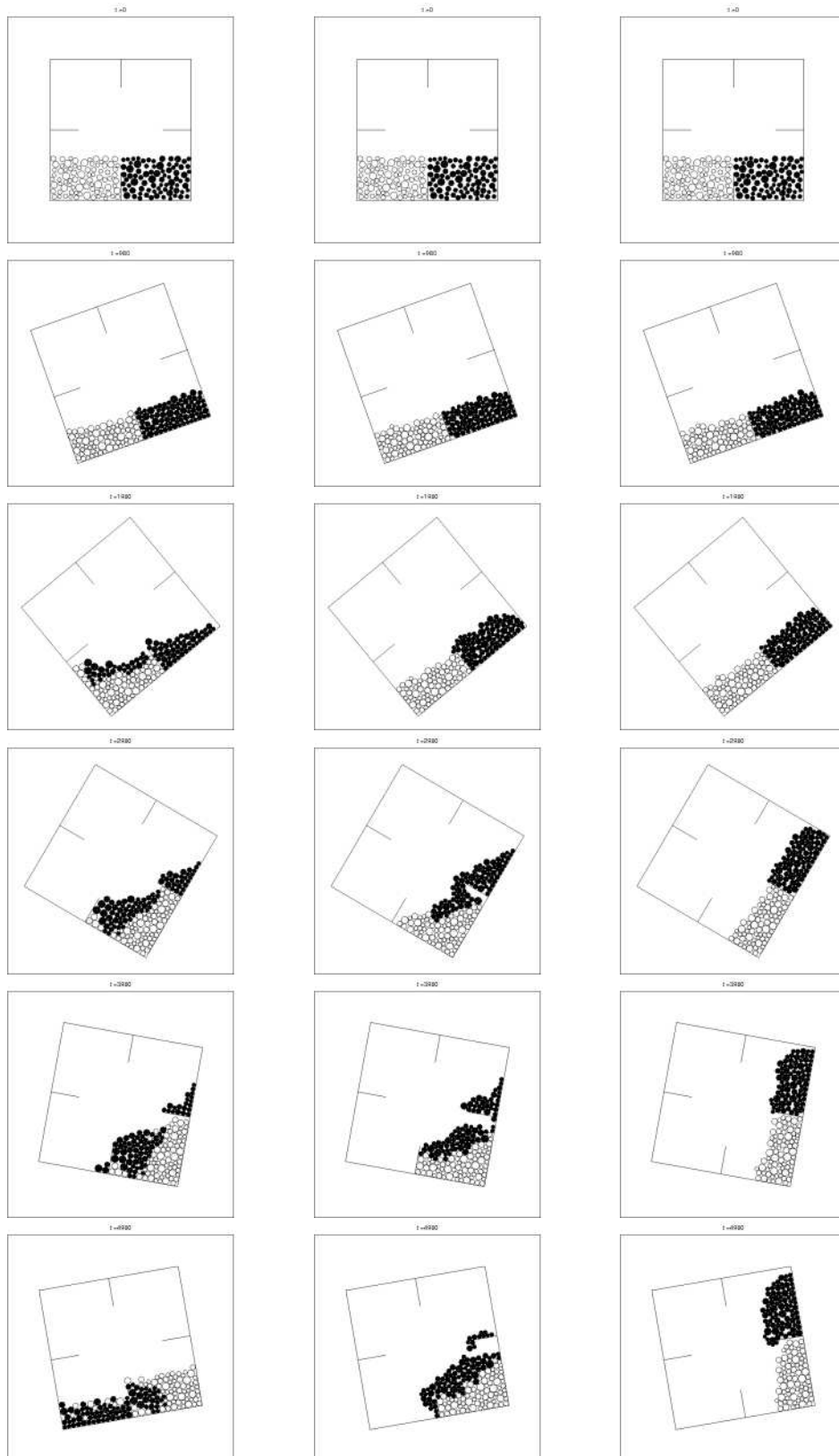


FIGURE 12. Gluey lotto: configurations at different time-steps for $\gamma_{min} = 0$ on the left (inelastic contacts), $\gamma_{min} = -1$ in the middle (gluey rough particles) and $\gamma_{min} = -\infty$ on the right (gluey smooth particles).

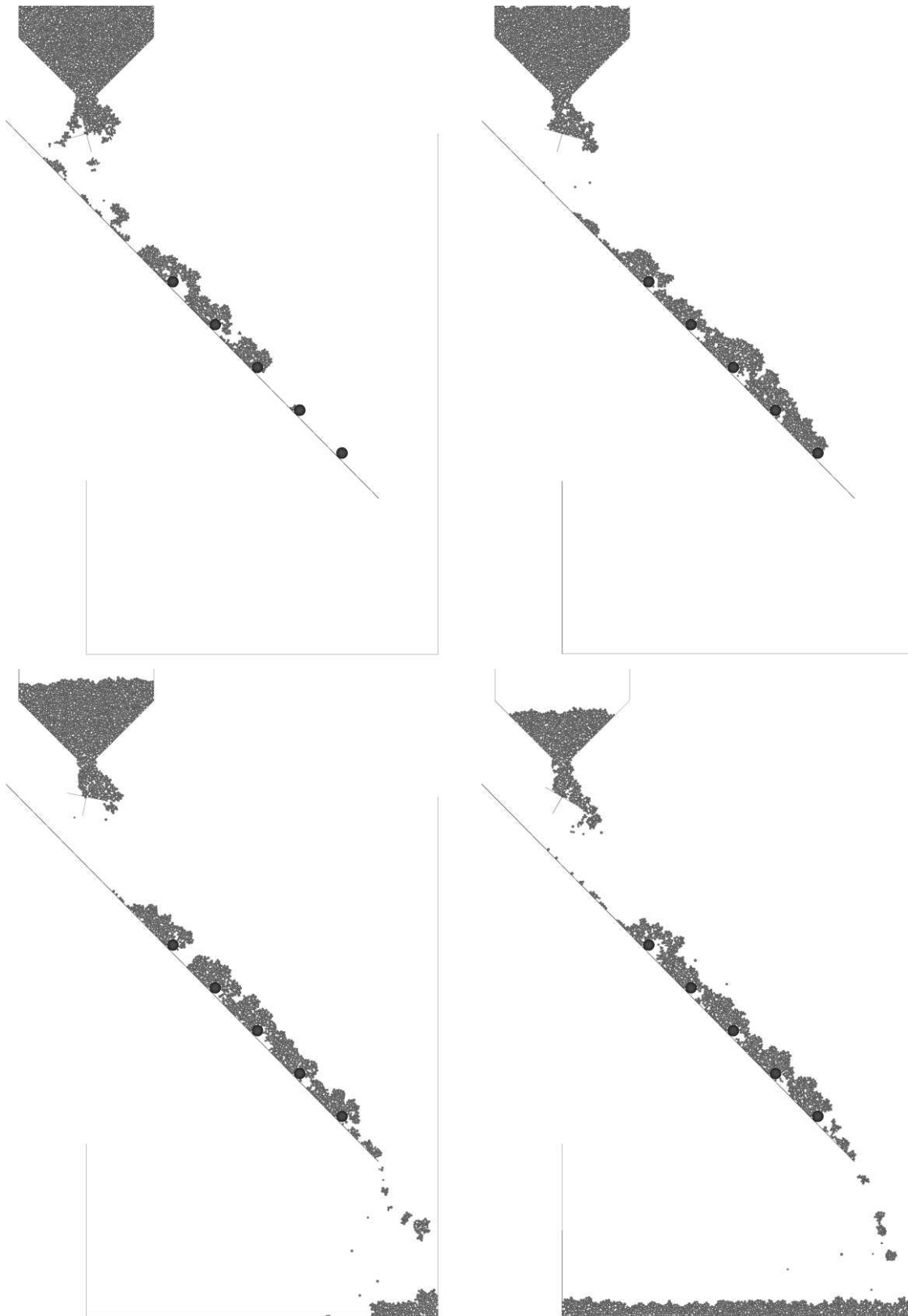


FIGURE 13. Snapshots of a two-dimensional simulation, 3000 particles: configurations at time-steps $n = 8826 - 14226$ (top) and $n = 18726 - 30726$ (bottom).

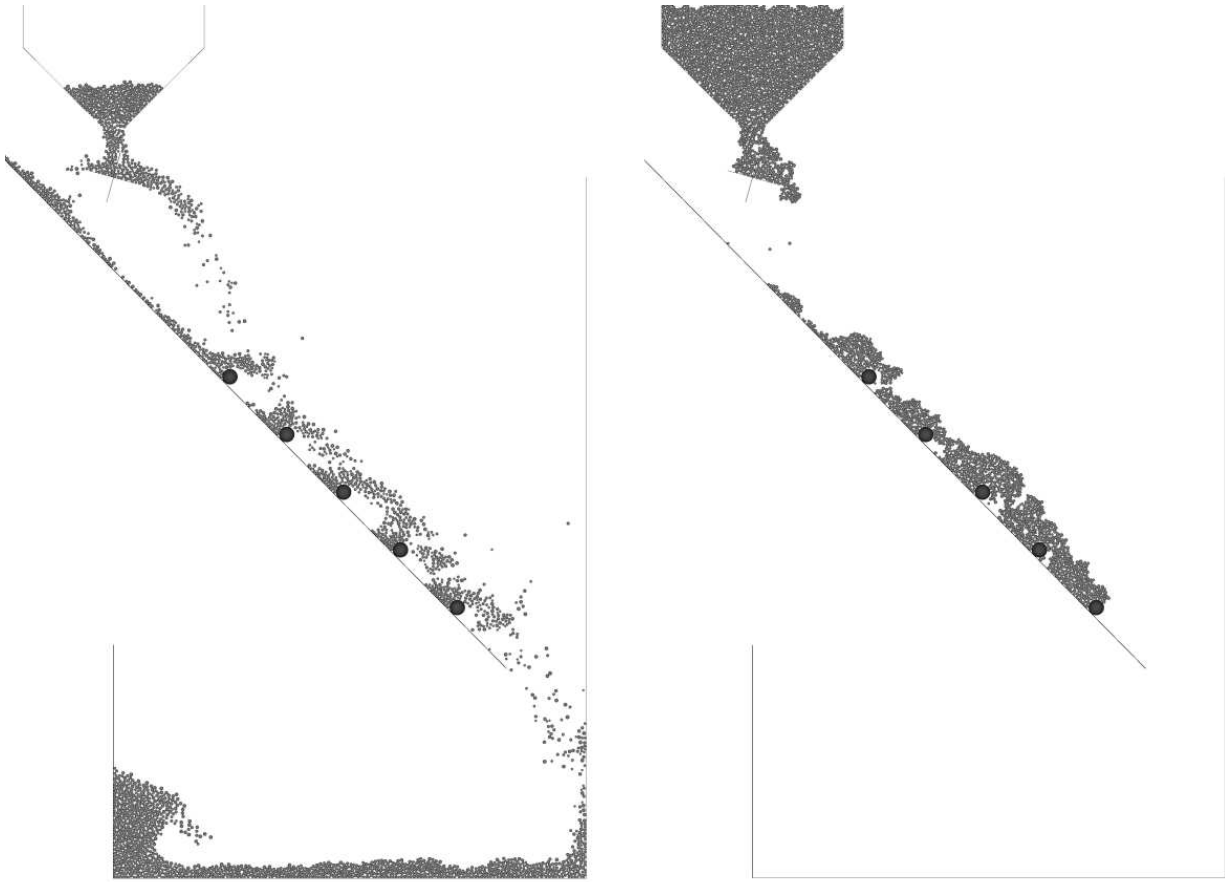


FIGURE 14. Snapshot of two-dimensional simulations, 3000 particles: dry (left) and viscous (right) simulations at time-step $n = 14226$.

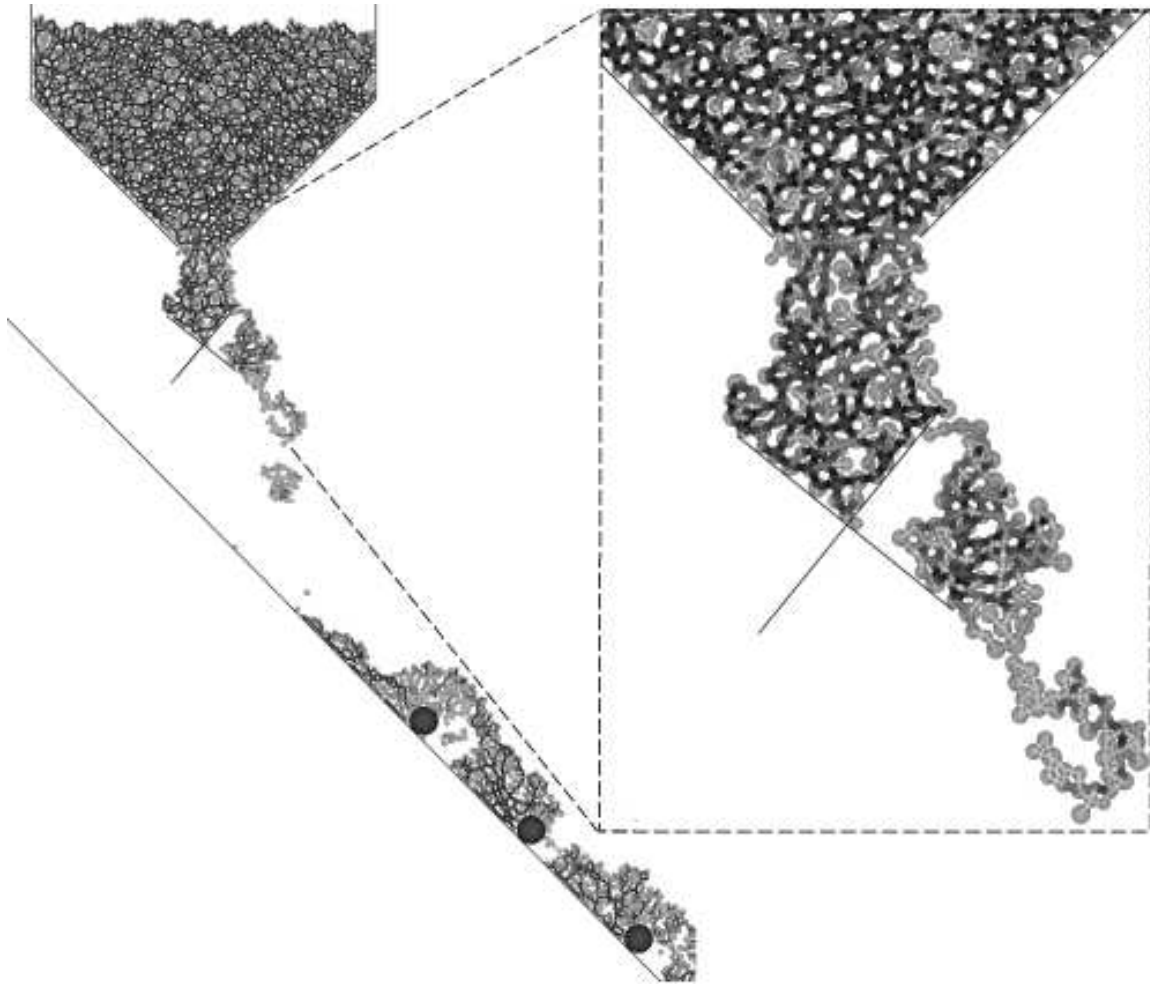


FIGURE 15. Snapshot of a two-dimensional gluey simulation, 3000 particles: configuration and values of γ at time-step $n = 14226$.

REFERENCES

- [1] R.G. Cox and H. Brenner, *The slow motion of a sphere through a viscous fluid towards a plane surface - II - Small gap width, including inertial effects*, Chem. Engng. Sci., Vol.22, pp.1753-1777, (1967)
- [2] R.G. Cox, *The motion of suspended particles almost in contact*, Int. J. Multiphase Flow, Vol.1, pp.343-371, (1974)
- [3] S.L. Dance and M.R. Maxey, *Incorporation of lubrication effects into the force-coupling method for particulate two-phase flow*, J. Comp. Phys., Vol.189, pp.212-238, (2003)
- [4] B. Desjardin and M.J. Esteban, *Existence of weak solutions for the motion of rigid bodies in a viscous fluid*, Arch. Ration. Mech. Anal., Vol.146(1), pp.59-71, (1999)
- [5] A. Einstein, Ann. Phys. Leipsig, Vol.19, p.289, (1906), Ibid. Vol.34, p.591, (1911)
- [6] E. Feireisl, *On the motion of rigid bodies in a viscous incompressible fluid*, J. Evol. Equ., Vol.3(3), pp.419-441, (2003)
- [7] R. Glowinski and T-W. Pan and T.I. Hesla and D.D. Joseph, *A distributed lagrange multiplier/fictitious domain method for particulate flows*, Int. J. Multiphase Flow, Vol.25, pp.755-794, (1999)
- [8] F. Hecht and O. Pironneau, <http://www.freefem.org>
- [9] M. Hillairet, *Lack of collision between solid bodies in a 2D constant-density incompressible viscous flow*, accepted in Communication in Partial Differential Equations.

- [10] H.H. Hu, *Direct simulation of flows of solid-liquid mixtures*, Int. J. Multiphase Flow, Vol.22(2), pp.335-352, (1996)
- [11] A.A. Johnson and T.E. Tezduyar, *Simulation of multiple spheres falling in a liquid-filled tube*, Comput. Methods Appl. Mech. Engrg., Vol.134, pp.351-373, (1996)
- [12] S. Labbé, J. Laminie and V. Louvet, *CSiMoon. Calcul scientifique, méthodologie orientée objet et environnement : de l'analyse mathématique à la programmation*, Technical report RT 2001-01, Laboratoire de Mathématiques, Université Paris-Sud, (2004)
- [13] A. Lefebvre, *Fluid-Particle simulations with FreeFem++*, ESAIM:Proc, Jean-Frédéric Gerbeau & Stéphane Labbé, Editors, Vol.18, pp.120-132, (2007)
- [14] A. Lefebvre, *PHD thesis*, Université Paris-Sud XI, Orsay, France, (2007)
- [15] A. Lefebvre, <http://mahery.math.u-psud.fr/~lefebvre/SCoPI.htm>
- [16] B. Maury, *A many-body lubrication model*, C.R. Acad. Sci. Paris, Vol.325(I), pp.1053-1058, (1997)
- [17] B. Maury, *Direct simulation of 2D fluid-particle flows in bi-periodic domains*, J. Comp. Phys., Vol.156, pp.325-351, (1999)
- [18] B. Maury, *A time-stepping scheme for inelastic collisions*, Numerische Mathematik, Vol.102(4), pp.649-679, (2006)
- [19] B. Maury, *A gluey particle model*, ESAIM:Proc, Jean-Frédéric Gerbeau & Stéphane Labbé, Editors, Vol.18, pp.133-142, (2007)
- [20] S. Naseri and N. Phan-Thien and X.J. Fan, *Lubrication approximation in completed double layer boundary element method*, Computational Mechanics, Vol.26, pp.388-397, (2000)
- [21] N.A. Patankar and P. Singh and D.D. Joseph and R. Glowinski and T-W. Pan, *A new formulations for the distributed lagrange multiplier/fictitious domain method for particulate flows*, Int. J. Multiphase Flow, Vol.26, pp.1509-1524, (2000)
- [22] J.A. San Matión, V. Starovoitov and M. Tucsnak, *Global weak solutions for the two-dimensional motion of several rigid bodies in an incompressible viscous fluid*, Arch. Ration. Mech. Anal., Vol.161(2), pp. 113-147, (2002)
- [23] P. Singh and T.I. Hesla and D.D. Joseph, *Distributed lagrange multiplier method for particulate flows with collisions*, Int. J. Multiphase Flow, Vol.29, pp.495-509, (2003)
- [24] T. Takahashi, *Analysis of strong solutionss for the equations modeling the motion of a rigid-fluid system in a bounded domain*, Adv. Differential Equations, Vol.8(12), pp.1499-1532, (2003)
- [25] T. Takahashi, *Existence of strong solutions for the problem of a rigid-fluid system*, C.R. Math. Acad. Sci. Paris, Vol.336(5), pp.453-458, (2003)
- [26] O.I. Vinogradova and G.E. Yacubov, *Surface roughness and hydrodynamic boundary conditions*, Phys. Rev. E, Vol.73, 045302(R), (2006)
- [27] D. Wan and S. Turek, *Direct numerical simulation of particulate flow via multigrid FEM techniques and the fictitious boundary method*, Vol.51, pp. 531-566, Int. J. Numer. Meth. Fluids (2006)